

EXPERIMENTAL AND CFD STUDIES OF FAT FOULING IN A NOVEL SPINNING DISC SYSTEM

R.Y. Nigo¹, Y.M.J. Chew^{1*}, N.E. Houghton², W.R. Paterson¹ and D.I. Wilson¹

¹ Department of Chemical Engineering and Biotechnology, University of Cambridge, New Museums Site, Pembroke Street, Cambridge CB2 3RA, UK

² Department of Engineering, University of Cambridge, Trumpington Street, Cambridge, CB2 1PZ, UK

*corresponding author: ymjc2@cam.ac.uk

ABSTRACT

Fats, like waxes, can cause freezing fouling when subjected to temperatures below their cloud point, both in heat exchangers and during transport of mixtures along pipelines in factories where it is termed 'coring'. This paper reports the use of a novel spinning disc apparatus (SDA) to study freezing fouling from fat mixtures, here a model solution of tripalmitin in a non-crystallising paraffin oil. The SDA employs smaller volumes of solution than conventional flow cell loops, is simple to operate, allows the fouled surface to be recovered, and features well-defined flow conditions.

For this application the device operates in the laminar regime, allowing computational fluid dynamics (CFD) simulations to elucidate the heat transfer and flow behaviour in the system, with particular focus on the heat flux and the shear stresses imposed on the surface. The CFD results showed good agreement with experimental heat transfer measurements.

The scope of the device is demonstrated with a short experimental study of PPP deposition from 10 wt% solutions on smooth stainless steel surfaces.

INTRODUCTION

Fouling of heat transfer and other process equipment surfaces is a problem in many industries, and can be particularly severe in the food sector where the materials being processed contain components such as proteins, fats and mineral salts that are precursors for the build-up of fouling layers. Such deposits reduce the efficiency of process units and incur costs via extra cleaning to avoid cross-contamination among products, or to maintain hygiene and microbial security (Fryer *et al.*, 1997).

Epstein (1983) classified fouling according to the mechanisms of deposit formation, and identified two variants of crystallisation fouling, determined by the solubility behaviour: *scaling* – associated with inverse solubility salts such as calcium carbonate and phosphate in heating aqueous systems, and *freezing fouling* – where cooling the fluid induces solidification. Most of the work on freezing fouling has concentrated on petroleum blends where cooling induces solidification of waxes and is indeed

exploited in the manufacture of lubricants. Examples of recent work in wax fouling include those by Akbarzadeh and Zougari (2008), Parthasarathi and Mehrotra (2005) and Singh *et al.* (2001). Significant advances in the understanding of kinetics of wax formation and ageing have been achieved and models developed for scaling up experimental results and predicting operating scenarios.

Fouling phenomena analogous to wax deposition are experienced in the food sector, where liquid and semi-crystallised mixtures of fats are used in large quantities in baking and biscuit manufacture. Large quantities of fat mixtures are prepared in a central facility and transported to the point of use, e.g. mixers. Food fats are mixtures of triglycerides and smaller quantities of diglycerides and, like waxes, can cause freezing fouling when subjected to temperatures below their cloud point, T_c , so that deposits can build up on pipe walls. This *coring* occurs via crystallisation, and yields a viscous gel which can harden to give a solid deposit over time. The impact of coring includes impairing the thermal and hydraulic efficiencies of the equipment. Relatively little work has been reported on food fat fouling: Fernandez-Torres *et al.* (2001) reported a modelling approach including a fouling regime map using concepts taken from wax deposition in crude oil pipelines. Fitzgerald *et al.* (2004) studied fouling utilising a model fat solution prepared out of a single crystallising component, tripalmitin (PPP), in a non-crystallising paraffin solvent using a flat plate heat exchanger. PPP is often used as a model fat because it arises in many vegetable and food fat blends, and the melting point of pure PPP, at approximately 63°C, means that deposition can be studied with coolants operating near ambient temperature.

This paper extends the experimental investigations of Fitzgerald *et al.* using similar model solutions but using a novel test configuration, the spinning disc apparatus (SDA). The two most common techniques reported in the literature for studying the fouling behaviour of waxes in crude oil are the flow cell loop (*e.g.* Ghedamu *et al.*, 1997) and the cold finger (*e.g.* Jennings and Weispfennig, 2005). In the former, warm oil (above its cloud point) flows along a long duct – often a pipe – with cooled walls so that the wax solidifies on the wall. The volumes of fluid and size of apparatus are

found to be similar to T_{cw2} and T_{cw3} , *i.e.* $\sim \pm 0.5$ K, so the coolant temperature, T_{cw} , was taken to be T_{cw1} . The values of T_{b1} and T_{b2} were similar, *i.e.* $\sim \pm 0.5$ K, and their arithmetic mean was used as the average bulk temperature, T_b .

The warm solution is held at a temperature, T_b , above its cloud point, and is in contact with an initially clean cool outer wall surface at temperature $T_{ss,out} < T_c$. Solution at the wall will be locally saturated and form crystals: deposition generates an insulating fouling layer, with solid-liquid interface temperature, T_s , initially close to $T_{ss,out}$ but gradually increasing and approaching T_b as deposit builds up. If T_s reaches T_c the solution at the interface will be too warm for crystallisation. The solid-liquid interface temperature T_s can be calculated from measurements of the heat flux (explained later).

The local heat flux through the rotating disc, q , is given by Newton's law of cooling:

$$q = U(T_b - T_{cw}) = h_b(T_s - T_b) \quad (1)$$

where h_b is the film heat transfer coefficient on the solution side and U is the overall heat transfer coefficient, calculated from:

$$\frac{1}{U} = R_{cw} + R_w + \frac{\delta_f}{\lambda_f} + \frac{1}{h_b} = R_{else} + \frac{\delta_f}{\lambda_f} + \frac{1}{h_b} \quad (2)$$

Here, δ_f and λ_f are the thickness and thermal conductivity of the fouling deposit; R_{cw} and R_w are the resistance to heat transfer on the coolant side and through the base plate(s), respectively. Both of the latter terms are expected to remain constant during a fouling experiment, while R_{cw} is expected to be weakly related to rotational speed owing to the strong influence of the jet on the flow pattern within the can. Table 1 summarises the thermal resistance of the fixed components in the heat transfer configuration.

Table 1: Heat transfer properties of components.

Material	λ (W/m K)	δ (m)	R (m ² K/W)
Brass	109	0.009	0.83×10^{-4}
Stainless steel	16	0.004	2.45×10^{-4}
Heat flux sensor	n/a	negligible	5.00×10^{-4}
Coolant	0.58 – 0.64	-	$\geq 50.0 \times 10^{-4}$
PPP deposit/ bulk paraffin	0.15	varies	varies

The value of R_w , at approximately 8.3×10^{-4} m²K/W, corresponds to heat conduction through a paraffin layer of thickness 6 μ m: R_w is not, therefore, expected to be a controlling factor in heat transfer.

Model solutions

Heat transfer experiments utilised liquid paraffin (density at 20°C, 855 kg/m³), which was used as the solvent in the model solutions. Tripalmitin, PPP, was obtained as 90% pure and dissolved in paraffin to give 10 wt% solutions. The apparent viscosity was measured using a Bohlin CV120 controlled stress rheometer with 50 mm parallel plates and found to be independent of PPP

concentration above the cloud point. The data were found to follow a temperature dependency of the form

$$\mu_b = 375.74 \exp(-0.031T) \quad (3)$$

where T is in Kelvin.

The cloud point of solutions was measured using a test apparatus similar to that reported by the European Oleochemicals and Allied Products Group (1987) and yielded a T_c value of 37°C for the 10 wt% solution used in these fouling tests.

The freezing point of the PPP was measured using a Pyris 1 DSC (Perkin Elmer, UK) fitted with a refrigeration intercooler. The value obtained, of 61.8°C, compared favourably with the trend in data reported by Fitzgerald *et al.* (2004), of 63°C for 95 wt% PPP and 65 °C for 99 wt% PPP. The melting points of the solutions were also measured using DSC. The melting points of solutions across the range 2-30 wt% PPP were consistently higher (by *c.* 12 K) than their corresponding T_c values, and could be described by the solid-liquid equilibrium relationship expected for an ideal solution and pure solid as described by Atkins (1997).

The deposits formed during fouling could be recovered and analysed. For instance, the rheology was characterised using a Bohlin CV120 controlled stress rheometer and the particle distribution and size by scanning electron microscopy and laser scattering. Details of the characterisation methods are given in Nigo (2008).

Experimental methods

The reservoir was charged with 2 L of the test solution and heated to the desired bulk temperature by circulating hot water through the heating jacket and mixed by a magnetic stirrer. The cooled can was initially isolated from the reservoir and brought to the required temperature by circulation of coolant. A support frame was constructed to hold the can and motor assembly horizontal before and after immersion. Once temperatures had equilibrated, condensate was removed from the can assembly, the disc cleaned with hexane and dried. The can was then immersed in the solution and rotation started. It was important at this point to inspect the disc surface visually for air bubbles, as these can affect heat transfer and deposition. Air bubbles could usually be displaced by increasing the rotation speed.

Two sets of experiment were performed, termed *heat transfer tests* and *fouling studies*.

Heat transfer tests. The main purpose here was to test the heat transfer performance and operability of the unit. The results were compared with CFD simulations. These experiments were performed using liquid paraffin with temperature driving forces, $\Delta T = T_b - T_{cw}$, ranging from 17-52 K, and rotational speeds, ω_b , from 3-60 rpm. Heat flux and temperatures were recorded over 30 minutes to ensure that any transients had been eliminated. The effect of ΔT was investigated with T_b held constant, at 60°C, while T_{cw} was varied between 8 and 43°C at a can rotation speed of 60 rpm. The effect of ω_b was studied at $\Delta T = 28$ K with $T_b = 50^\circ\text{C}$ and $T_{cw} = 22^\circ\text{C}$.

Fouling tests. Fouling tests reported here were conducted with 10 PPP wt% solutions at $T_b = 50^\circ\text{C}$. The coolant temperatures used were 2°C , $(T_c - 5)$ K, and $(T_c - 15)$ K. The lowest value, 2°C , reflects winter conditions in the UK and can be readily generated in a laboratory chiller over extended periods, whilst the latter values represent different degrees of subcooling. Rotational speeds used were 3, 33 and 60 rpm, corresponding to Reynolds number, Re_r , values of 11, 118 and 215, respectively. The Reynolds number is defined as

$$Re_r = \frac{4\rho\omega_d r_d^2}{60\mu} \quad (4)$$

where r_d is the radius of the disc and the physical properties are evaluated at the film temperature. The experimental conditions used in the tests are summarised in Table 2.

Table 2: Summary of experimental conditions.

	Heat transfer	Fouling
Coolant temperature, T_{cw}	17 – 52°C	2°C, $(T_c - 5)$ $(T_c - 15)$
Bulk temperature, T_b (°C)	60	50
PPP concentration, (wt%)	0	10
Rotational speed, ω_d (rpm)	3 - 60	3, 33, 60

Temperatures and heat fluxes were monitored over a fouling test. At the end of the test, the rotation was stopped and the can assembly lifted off the main unit, placed on the support frame and left standing for about 2 minutes to allow excess solution to drip off the test plate. The gel formed on the test plate, including residual solution held by surface tension, was then carefully scraped off using a plastic spatula, weighed and stored for analysis.

The amount of residual solution could be significant so a blank run was performed after each fouling test to determine how much liquid remains on the fouling cell plate as a result of surface tension. The test plate was cleaned thoroughly, the can lowered into the reservoir and rotated at the experimental conditions for one minute before withdrawing it and resting it on the support frame for 1-2 minutes. Liquid adhering to the test plate was removed and weighed. This amount was subtracted from the measured fouled mass to give the true deposit mass.

It should be noted that fouling tests could last 24 h or longer and a small number of tests were repeated in order to gauge the reproducibility of the approach. These displayed good agreement so tests were thereafter only repeated when the results were inconsistent with observed trends.

NUMERICAL SIMULATIONS

Laminar flow about a rotating disc immersed in a large body of quiescent fluid was first studied by von Kármán (1921). Surface temperature and the shear stress acting on the disc surface are key parameters in freezing fouling. The commercial finite element method (FEM) software COMSOL MULTIPHYSICS™ (version 3.5, Chemical Engineering Module), was used for simulating the fluid flow and heat transfer behaviour of pure paraffin liquid in the SDA, *i.e.* simulating the *heat transfer* experiments, and are

compared with experimental measurements of heat flux. Simulations of *fouling* experiments were not attempted.

The flow-field is simulated by solving the continuity equation and the axisymmetric, incompressible, steady state Navier-Stokes (NS) equation for a Newtonian liquid. All flows are laminar. The steady state energy equation with no heat source or heat sink can be written as:

$$\rho_b C_{p,b} (\mathbf{v} \cdot \nabla T) = \nabla \cdot (\lambda_b \nabla T) \quad (5)$$

where T is the temperature, $C_{p,b}$ the bulk specific heat capacity and λ_b the bulk thermal conductivity. Physical properties such as density, thermal conductivity and specific heat did not change significantly with temperature and are assumed constant. The temperature dependence of the dynamic viscosity is incorporated and was modelled by Eqn. (3). The physical and thermal properties used in the simulations are summarised in Table 3.

Table 3: Summary of parameters used in CFD simulations.

Parameters	Value
Radius of disc, r_d	0.04 m
Bulk temperature, T_b	50°C
Coolant temperature, T_{cw}	22°C
Rotational speed of can, ω_d	3 - 60 rpm
Apparent viscosity of bulk, μ_b	(2°C): 0.040 kg/m s (50°C): 0.016 kg/ms
Density of bulk, ρ_b	855 kg/m ³
Thermal conductivity of bulk, λ_b	0.15 W/m K
Specific heat capacity of bulk, $C_{p,b}$	2107 J/kg K
Rotational speed of stirrer, ω_{mag}	- 2.0 rad/s

The physical configuration is cylindrically symmetric and the geometry of the model is illustrated in Fig. 3. Axisymmetry allows considering the computational domain as half of the system to be modelled. The mesh contains approximately 5000 triangular elements, with a higher concentration of elements at the boundary between the disc and the liquid (approximately five times greater than the other boundaries). The number of elements was optimized by performing a series of simulations with different mesh sizes, starting from a coarse mesh and refining it until the results were mesh-independent. A converged solution took approximately 15 min on a desktop PC with a 3.16 GHz dual core processor and 3.33 GB RAM.

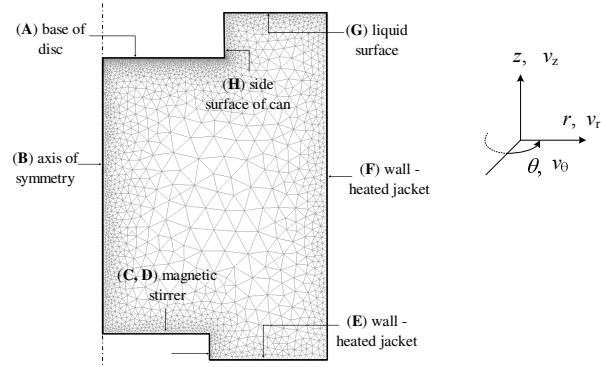


Fig. 3: FEM mesh of the simulation domain showing boundary labels (A-H). The darkness of the areas in the figure indicates the density of the mesh.

Convergence was assessed by comparing the values of velocity and temperature from successive iterations; tolerances were set at 10^{-5} m/s (versus a lowest mean tangential velocity of the cooling can of 1.3×10^{-2} m/s) and 10^{-5} K (versus a lowest coolant temperature of 2°C), for the velocity and temperature, respectively. The tolerance dictates the error in each iteration.

The quantitative information specified for each simulation is the rotational speed of the can, ω_d , that of the magnetic stirrer, ω_{mag} , and the temperatures of the coolant, T_{cw} , and the bulk warm solution, T_b . The outputs of the CFD calculation are the velocity field and temperature profile. The latter allows the heat flux across the region of the rotating disc beneath the heat flux sensor in the experimental apparatus (Fig. 2) to be calculated and compared with experimental data.

The boundaries are labelled (A-H) on Fig. 3 and are subject to the following conditions:

(A) **Base of disc:** Uniform temperature: the surface temperature, $T_{\text{ss,out}}$, is assumed to be the coolant temperature, T_{cw} . It is shown, later, in Fig. 7 that the resistance for the base plates, R_w , is small compared to the thermal resistances of the bulk, R_b , and coolant, R_{cw} . Therefore, it is reasonable to assume that the temperature of the disc is uniform. The boundary is impermeable and the rotational speed is specified via

$$v_\theta = \omega_d r \quad (6)$$

where v_θ is the velocity component in the azimuthal direction and r the radial coordinate.

(B) **Axis of symmetry:** There is no fluid or thermal energy flow across the line of symmetry, so it is adiabatic.

(C, D) **Magnetic stirrer:** This boundary is adiabatic and impermeable. The rotational speed is specified, at

$$v_\theta = -\omega_{\text{mag}} r \quad (7)$$

(E, F) **Wall-heated jacket:** The inner wall temperature is specified, at T_b , the temperature of the solution. The boundary is impermeable and there is no slip at the wall.

(G) **Liquid surface:** There is little heat loss from the liquid surface, so is treated as adiabatic. This free surface is modelled with slip conditions:

$$v_z = 0 \quad \text{and} \quad v_\theta = 0 \quad (8)$$

where v_z is the velocity component in the axial direction.

(H) **Side surface of can:** The wall is insulated so is treated as adiabatic, with rotational speed given by Eqn. (6).

RESULTS AND DISCUSSION

Heat transfer

Fig. 4 shows a sample set of experimental data from the heat transfer experiments. The heat flux is linearly proportional to the temperature driving force ($\Delta T = T_b - T_{\text{cw}}$), as expected, and the overall heat transfer coefficient, U_{exp} , can be extracted from the regression line.

The effect of dimensionless disc speed, Re_r , on heat flux at fixed ΔT (and therefore U) is presented in Fig. 5. The fitted trend line shows that the heat flux varies with $Re_r^{0.51}$,

indicating that the overall heat transfer coefficient, U_{exp} , is roughly proportional to $\omega_d^{1/2}$.

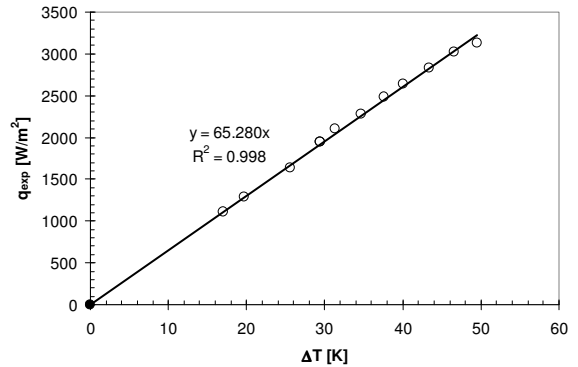


Fig. 4: Effect of temperature driving force, ($\Delta T = T_b - T_{\text{cw}}$), on measured heat flux. Conditions: liquid paraffin at 50°C , $\omega_d = 5.2$ rad/s (50 rpm) and $\omega_{\text{mag}} = -2.0$ rad/s. Symbol size reflects experimental uncertainty. Solid line shows regression fit.

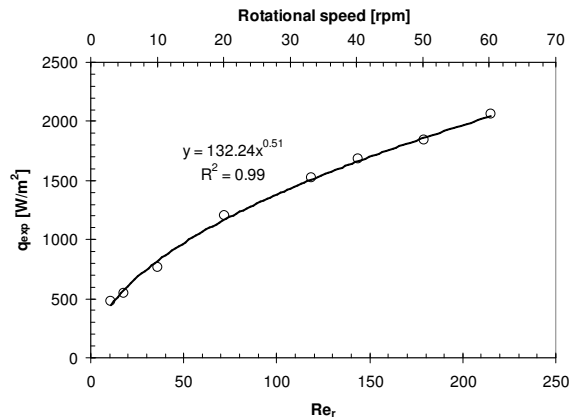


Fig. 5: Effect of Reynolds number, Re_r , on heat flux. Locus shows line of best fit for simple power law model. Conditions: liquid paraffin, $T_{\text{cw}} = 22^\circ\text{C}$, $T_b = 50^\circ\text{C}$ and $\omega_{\text{mag}} = -2.0$ rad/s.

A similar relationship was obtained by Sparrow and Gregg (1959), in their investigations of the heat transfer characteristics of rotating discs located in a large pool of quiescent liquid. These results indicate that the SDA is operating in the laminar regime and that the conditions employed in the experiments did not exceed the sensor sensitivity.

CFD simulations

The CFD simulation predicts the velocity and temperatures distributions in the liquid in the heat transfer experiments. Mass transfer, which can also be involved in limiting fouling, is not considered but could be readily included. Fig. 6 shows the temperature profiles (coloured map) and flow patterns (contour lines) for a set of simulations at can rotational speeds employed in the experiments reported in Fig. 5. Two vortices are evident in the bulk liquid: an upper one driven by the rotation of the can and a lower one induced by the magnetic stirrer acting in the opposite direction. As the magnetic stirrer speed is

kept constant, increasing the can speed increases the size of the upper recirculation zone, as expected. It is also evident that the rotational speed has an effect on the flow patterns and thus the temperature profiles. At high can speeds, *i.e.* > 10 rpm, the temperature of almost the entire domain approaches that of the bulk. Note that CFD validation is not presented in this work as there is no single parameter that allows direct comparison using the current setup. However, the use of particle imaging velocimetry to study the flow patterns of the bulk solution is planned and this will allow us to confirm the flow field predictions.

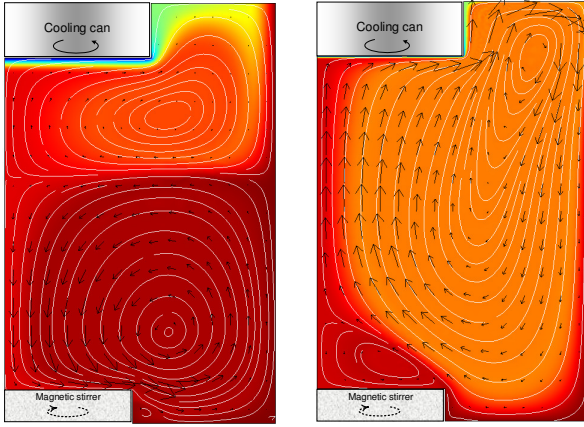


Fig. 6: Flow patterns and temperature profiles in the SDA for can rotational speeds of 3 rpm (left) and 60 rpm (right). Black arrows are velocity vectors. Shading indicates temperature, with 50°C – dark red, 22°C – dark blue.

The film heat transfer coefficient on the bulk side, $h_{b,sim}$, can be calculated from the temperature profiles and these are compared with the overall heat transfer coefficient, U_{exp} , obtained from experiments. The $h_{b,sim}$ values were consistently larger than the U_{exp} values, which is expected as the latter includes the resistances across the can and coolant. The latter resistance, $R_{else} (=R_{cw} + R_w)$, can be estimated from $(1/U_{exp} - 1/h_{b,sim})$, according to Eqn. (1), and the results are plotted in Fig. 7.

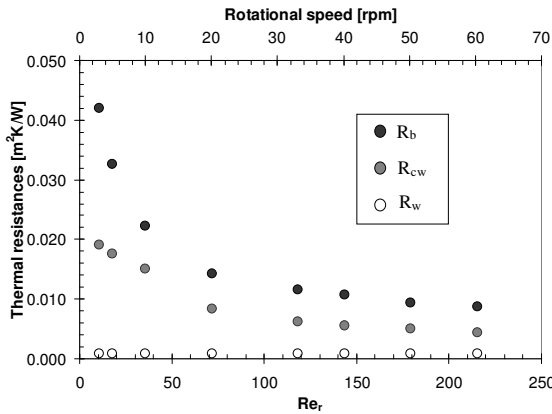


Fig. 7: Thermal resistances in the SDA apparatus: $R_b (=1/h_{b,sim})$, R_w and $R_{cw} (=R_{else} - R_w)$.

Both resistances decrease with increasing Re_r , and R_b is consistently larger than R_{else} at all rotational speeds,

indicating that the dominant resistance to heat transfer lies on the solution side. R_{else} varies from 0.02 m²K/W to 0.006 m²K/W, which is noticeably greater than the estimated value of R_w , of 0.00082 m²K/W (Table 1), suggesting that the coolant side resistance, R_{cw} , is significant. This also implies that wall resistances play a minor part and the assumption that the wall is at uniform temperature is reasonable. Rotation speed has a larger effect on R_b than R_{cw} , which is expected as the coolant flow is also determined by the internal circulation in the can. The flow field within the can was not simulated as initial estimates of Reynolds numbers indicated that the flow lay in the turbulent regime, requiring extensive further computational effort.

The surface temperature of the disc in contact with the warm solution in fouling experiments (before fouling occurs) will be near, but not at, T_{cw} . Fig. 7 suggests that a working estimate of surface temperatures could be made using $R_{cw} \sim \frac{1}{2} \times R_b$ and assuming R_w being negligible, giving:

$$q = \frac{(T_{ss,out} - T_{cw})}{R_{cw}} = \frac{(T_b - T_{cw})}{(R_{cw} + R_b)} \quad (9)$$

$$\therefore T_{ss,out} = T_{cw} + \frac{\frac{1}{2}R_b}{\frac{1}{2}R_b + R_b}(T_b - T_{cw}) = \frac{2}{3}T_{cw} + \frac{1}{3}T_b \quad (10)$$

The shear rate and the shear stress imposed on the surface disc can also be calculated from the simulation velocity field. The shear stress distributions show that the maximum shear stress is found at the outer edge of the disc. The same trend was observed for shear rates and for all other temperature and rotational speeds investigated. Figure 8 shows the shear stress values at $r = 0.035$ m (the radius of the disc r_d is 0.040 m). It is also evident that the effect of rotational speed is greater than the effect of surface temperature.

The shear stresses imposed on the surface in the SDA device can be compared with those imposed by an oil in turbulent flow. For a bulk velocity of 1 m/s, an oil density of 800 kg/m³ and a Fanning friction factor of *c.* 0.005, this gives $\tau = \frac{1}{2} C_f \rho u^2$, ~ 2 Pa. This estimate suggests that information on fouling behaviour can be obtained at the laboratory scale in the SDA using relatively simple measurements under conditions relevant to industrial operation.

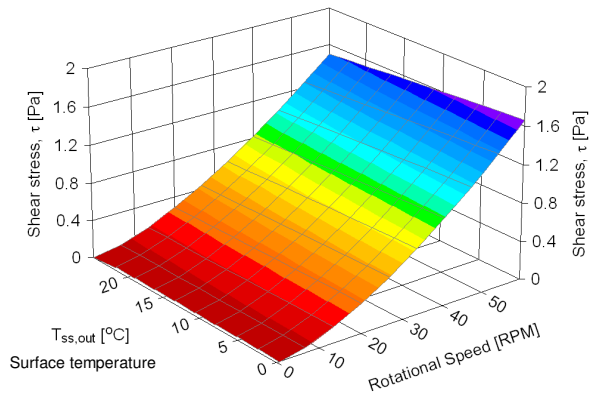


Fig. 8: Shear stress values on disc surface for different values temperatures and rotational speed at radial location $r = 0.035$ m.

Fouling experiments

Results presented here are primarily the mass of deposit formed, m_f , fouling resistance, R_f , and the inferred deposit thickness, δ_f . The reproducibility of fouling tests was confirmed by repeated tests with 10 wt% PPP solutions at $T_{cw} = 2^\circ\text{C}$ and $\omega_h = 3$ and 60 rpm ($Re_r = 11, 215$). The data in Fig. 9 show agreement within the bounds of experimental error, as well as noticeably different deposit mass-time profiles. At higher ω_h , *i.e.* 60 rpm, there is a short induction period followed by rapid growth up to 4 h, after which deposition was slow. At lower speed, 3 rpm, no induction period was observed, with 6 g of deposit formed after 1 h; deposit growth thereafter is slow, reaching a slightly larger final value than at 60 rpm after 24 h.

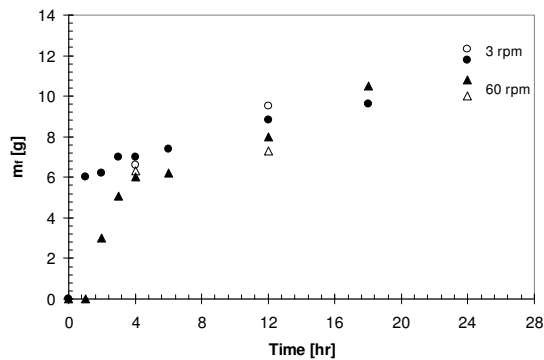


Fig. 9: Reproducibility of fouling runs. Conditions: $T_{cw} = 2^\circ\text{C}$, $T_b = 50^\circ\text{C}$: circles - 3 rpm, triangles - 60 rpm. The different symbols indicate separate runs.

The asymptotic or fouling rate behaviour observed is expected as the tests are performed under conditions of constant overall temperature driving force: as deposit accumulates, the deposit-solution interface temperature, T_s , will increase. Estimates of T_s for the profiles in Fig. 9 confirmed that T_s approached T_c at the end of the test.

The difference in behaviour between the high and low rotational speeds is elucidated by the heat transfer profiles in Fig. 10(a)–(c), which were obtained under similar conditions. The fouling resistance, R_f , shown in Fig. 10 (b), is calculated from

$$R_f = \frac{1}{U} - \frac{1}{U_o} \quad (10)$$

where U_o is the initial, clean, overall heat transfer coefficient. This is most readily estimated by extrapolating the q - t data back to $t = 0$, as the early values contain transients associated with the start of rotation. The heat fluxes obtained at the lower speed, *i.e.* 3 rpm, are 3-4 times smaller than those obtained at higher rotational speeds so contain more measurement scatter, but the data clearly show a sharp initial increase in R_f , mirroring that seen in the mass deposition measurements. This can be attributed to the formation of a weak gel on the surface due to the low temperature in the liquid which is able to resist removal as the shear induced by the rotation is low. This is not observed at higher rotational speeds because the shear stress

is large enough to shear off the weak gel formed at this temperature.

The deposit thickness profiles in Fig. 10(c) were estimated using

$$\delta_f = R_f \lambda_f \quad (11)$$

where the deposit thermal conductivity, λ_f , was taken to be 0.15 W/m K, as the thermal conductivity of solid PPP is conveniently close to that of the paraffin. The plots show a steady increase to a final thickness of 2-3 mm, which is consistent with visual observations and deposit volume.

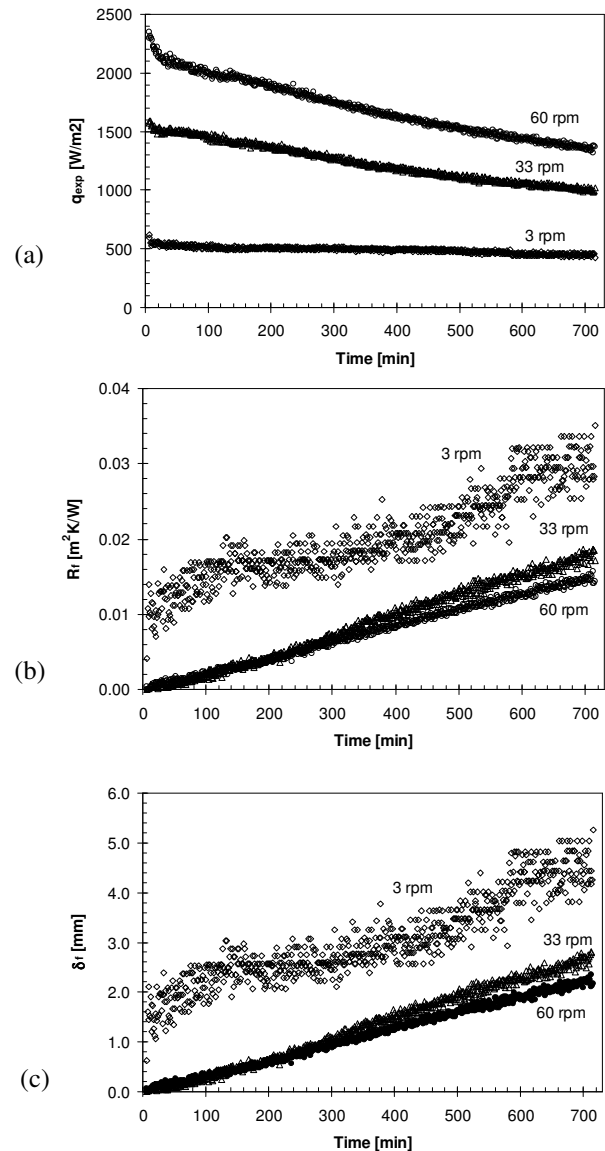


Fig. 10: Fouling of 10 wt% PPP solution: (a) heat flux, (b) fouling resistance and (c) estimated deposit thickness. Conditions: $T_{cw} = 22^\circ\text{C}$, $T_b = 50^\circ\text{C}$, $\omega_{mag} = -2.0$ rad/s.

Electron microscopy and X-ray analysis of the deposits confirmed that the PPP was crystallizing as pure needles of the β polymorph. The composition of the foulant was found to be strongly influenced by the surface conditions, particularly temperature and shear stress: at 3 rpm, the deposit was approximately 30 wt% PPP solids whereas at 60

rpm the solids content was closer to 60 wt%. These values indicate that the structure of the deposit varies and is determined by the physics of gelation. Separate rheometrical analysis of PPP-paraffin gels at 2 °C indicated that they exhibited 'yield-stress' behaviour, with a critical stress around 2-3 Pa, which is consistent with the shear stress values in Fig. 8. Further analyses and experimental studies are reported in Nigo *et al.* (2009).

CONCLUSIONS

1. A novel fouling apparatus, the SDA, has been developed for studying freezing fouling using moderate volumes of liquid. Fouling can be monitored in situ and samples readily recovered for analysis.
2. The laminar flows in the SDA in this freezing fouling application can be simulated using CFD techniques, yielding good agreement with heat transfer measurements and providing reliable estimates of surface conditions.
3. A preliminary investigation of freezing fouling using model solutions of PPP in paraffin highlighted the importance of gel formation conditions on fouling behaviour.

ACKNOWLEDGEMENTS

Financial support from the Association of Commonwealth Universities (UK) and the Papua New Guinea University of Technology for RYN, and funding for YMJC from the Royal Academy of Engineering are all gratefully acknowledged. Construction of the SDA was supported by a Food Processing Faraday Fast Track grant.

NOMENCLATURE

C_f	Fanning friction factor
C_p	specific heat capacity, J/kg K
g	gravitational constant, m/s ²
h	heat transfer coefficient, W/m ² K
m_f	mass of deposit, kg
q	heat flux, W/m ²
r	radial coordinate, m
R	thermal resistance, m ² K/W
Re_r	Reynolds number based on radius of rotating disc
T	temperature, °C or K
u	mean velocity, m/s
U	overall heat transfer coefficient, W/m ² K
v	velocity vector, m/s
z	axial coordinate, m
δ	thickness, m
λ	thermal conductivity, W/m K
μ	dynamic viscosity, kg/m s
θ	azimuthal coordinate, °
ρ	density, kg/m ³
τ	shear stress, Pa
ω	rotational speed, rad/s

Subscript

b	bulk
c	cloud point
cw	coolant
d	disc
else	everything else apart from bulk

exp	experiment
f	fouling deposit
o	initial
mag	magnet
w	combined setup of brass, heat flux sensor and stainless steel
s	surface of deposit in contact with bulk solution
sim	simulation
ss,out	outer surface of stainless steel disc

REFERENCES

- Akbarzadeh, K., and Zougari, M., 2008, Introduction to a novel approach for modeling wax deposition in fluid flows. 1 Taylor-Coutte system. *Ind. Eng. Chem. Res.*, Vol. 47, pp. 953-963.
- P.W. Atkins, 1997, *Physical Chemistry* (6th ed.), Oxford University Press, Oxford, UK.
- Epstein, N., 1983, Thinking about heat transfer fouling: A 5x5 matrix. *Heat Transfer Eng.*, Vol. 4(1), pp. 43-56.
- Fernandez-Torres, J.M., Fitzgerald, A.M., Paterson, W.R., and Wilson, D.I., 2001, A Theoretical study of freeze fouling: limiting behavior based on a heat and mass transfer analysis. *Chem. Eng. Proc.*, Vol. 40, pp. 335-344.
- Fitzgerald, A.M., Barnes, J., Smart, I., and Wilson, D.I., 2004, A model experimental study of coring by palm oil fats in distribution lines. *Food Bioprod. Process.*, Vol. 82, pp. 207-212.
- J.P. Fryer, D.L. Pyle and C.D. Rielly, 1997, *Chemical Engineering for the Food Industry*, Blackie Academic and Professional, London, UK.
- Ghedamu, M., Watkinson, A.P. and Epstein, N., 1997, Mitigation of wax oil build-up on cooled surfaces, in *Fouling Mitigation of Industrial Heat Exchange Equipment*, eds. Panchal, C.B., Begell House, NY, pp. 473-489.
- Grant, C.S., Perka, A.T., Thomas, W.D., and Caton, R., 1996, Cleaning of behenic acid residues from stainless steel. *AIChE J.*, Vol. 42, pp. 1465-1476.
- Jennings, D.W. and Weispfennig, K., 2005, Effects of shear and temperature on wax deposition: coldfinger investigation with a Gulf of Mexico crude oil. *Energ. Fuel.*, Vol. 19, pp. 1376-1386.
- Kármán, Th.Von, 1921, Uber laminare and turbulente. *Zeitschrift für Angewandte Mathematik und Mechanik*, Vol. 1, pp. 233-252.
- Nigo, R.Y., 2008, *Fouling behaviour of food fats*, PhD Dissertation, University of Cambridge, UK.
- Nigo, R.Y., Chew, Y.M.J., Houghton, N.E. Paterson, W.R. and Wilson, D.I. (2009) Experimental studies of freezing fouling of model food fat solutions using a novel spinning disc apparatus, *in preparation*.
- Parthasarathi, P., and Mehrotra, A.K., 2005, Solids deposition from multicomponent wax-solvent mixtures in a benchscale flow-loop apparatus with heat transfer. *Energ. Fuel.*, Vol. 19, pp. 1387-1398.
- Rashaida, A.A., Bergstrom, D.J., and Sumner, J.R., 2006, Mass transfer from a rotating disk to a Bingham fluid. *J. Appl. Mech.*, Vol. 109, pp. 108-111.
- Rosmaninho, R., and Melo, L.F., 2006, The effect of citrate on calcium phosphate deposition from simulated milk

ultrafiltrate (SMUF) solution, *J. Food Eng.*, Vol. 73(4), pp. 379-387.

Singh, P., Venkatesan, R., and Fogler, H.S., 2001, Morphological evaluation of thick wax Deposits during aging. *AIChE J.*, Vol. 47(1), pp. 1-18.

Sparrow, E.M. and Gregg, J.L., 1959, Heat transfer from a rotating disk to fluids of any Prandtl number. *J. Heat Trans.*, Vol. 81, pp. 249-251.